



# A PV generation system based on Incremental Conductance MPPT algorithm and SVPWM inverter for standalone applications

**Dhuha K. Khafz**<sup>1,a</sup>

<sup>1</sup> Communications Engineering Department, Iraq University College, Basrah - Iraq.  
E-mail: [Duhakareem249o0ll@gmail.com](mailto:Duhakareem249o0ll@gmail.com)

**Abstract.** Power produced at the output of photovoltaic (PV) Cells continues to change due to solar radiation and the surrounding environment temperature so that PV cells show non-linear characteristics of current and voltage. Therefore, the maximum power point of the solar cell relies on the amount of solar irradiation and environment temperature. Maximum Power Point Tracking (MPPT) technology is utilized in photovoltaic systems to take entire advantage of output power for Photovoltaic cells. This paper proposes an incremental conductance method MPPT algorithm that can simultaneously increase MPPT speed and accuracy. Inverter's controller is else important side of the Photovoltaic power generation system. This paper suggests a space vector pulse width modulation (SVPWM) control method of a 3-phase Pulse Width Modulation inverter is utilized in Photovoltaic power generation systems. A new stand-alone Photovoltaic generation system depended on the incremental conductance method MPPT algorithm with the space vector pulse width modulation control schema for 3-phase voltage source inverter is presented and structured into the Matlab / Simulink. Simulation results show the proposed stand-alone Photovoltaic system can achieve the excellent execution of MPPT and get the output voltage in high quality. The system is tested and varied using a solar cell Kyocera Solar KD215GX-LPU PV module.

**Keywords:** Photovoltaic system (PV) , Maximum PowerPoint Tracking (MPPT) ,Space vector pulse width modulation(SVPWM) ,DC-DC Boost Converter.

**Iraq University College Journal of Engineering and Applied Sciences** Volume 1, Issue 2

Received 10/09/2021

Accepted 20/11/2021

Published 20/12/2021

Online at <https://magazine.iuc.edu.iq/journal/>

DOI:yy.yyyy/ IUCJEAS.2021.xx.x.xx

## 1. Introduction

Because of the increasing demand for energy, pure, environmentally and sustainable energy is required. Solar energy, a type of renewable energy indicating a lot of interest in meeting growing load demands. Most of the solar energy sources that can be used to produce clean electricity are available for free everywhere, despite the cost of composition is high, the cost of operation is very low.[1].

Solar cells are variable current or voltage sources because they depend on the variation in temperature, irradiation, and load. Due to the solar cells have a low efficiency, Maximum power point tracking (MPPT) technology is utilized to supply the output of the solar cell effectively. The technology can source maximum power from different sources by utilizing a controlled DC-DC boost converter with a tracking algorithm inserted between the solar cell and the load [2]. MPPT technologies such as perturbation and observation (P&O), Incremental conductance (IC), and feedback linearization techniques are offered. In this paper, the IC Technique is used due to its low cost, easy implementation, and good execution [3].

In photovoltaic power generation systems, inverters that convert DC power from solar cells into AC power for grids are becoming more popular every day. Inverters are an important unit in the power regulation part of PV systems that use a variety of DC to AC converters. Inverter tasks in a power generation system including DC to AC conversion, system control, and output power quality assurance with various protection mechanisms [4]. Multi-level inverters with PWM control are becoming more important. They have many additional advantages over other topologies and extra efficient [5].

In previous research, Babaei et al.[6] proposed a new topology for a switched ZSI to achieve higher voltage gain than a conventional inverter. A sigma-Z-source topology was intended to achieve a higher dc-ac voltage gain with a smaller transformer. A better Pulse Width Modulation (PWM) approach was designed to reduce the switching frequency of a ZSI[8].

In this work, a structure of a photovoltaic generator system is proposed based on the IC algorithm and SVPWM technique for a 3-phase PWM inverter. The simulation result shows an increase in output power with better performance in output voltage and current.

## 2. Photovoltaic modelling

Solar cells convert the sun's rays into DC power. This is a physical process known as the photoelectric effect. A Photovoltaic array consists of multiple PV cells connected in parallel and in series to increase the voltage and current in the array. There are many types of solar cell modules. Describes a solar cell utilizing a single diode model, this can be designed by a current source anti-parallel to the diode, and parallel and series resistors are included for the ohm and leakage currents as shown in Figure 1[6]. In this paper, a solar cell module of the type Kyocera Solar KD215GX-LPU PV, in which the table parameter is listed below:

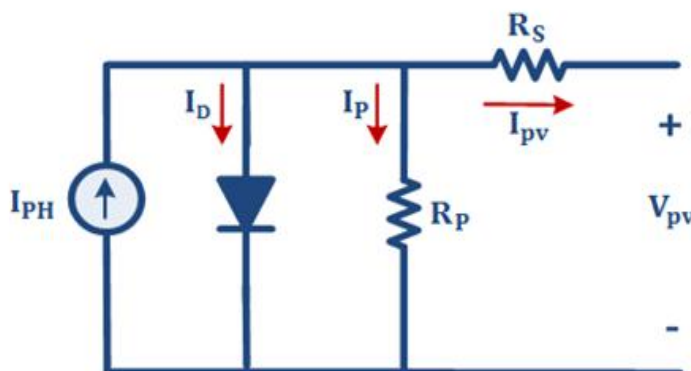


Fig. 1. The single-diode model

$$I_{PV} = I_{PH} - I_D - I_p \quad (1)$$

$$I_{PH} = I_p \frac{G}{1000} + K_i(T - T_{ref}) \quad (2)$$

$$I_0 = I_{do} \left( \frac{T}{T_{ref}} \right)^2 e^{\left[ \frac{qE_g}{nk} \left( \frac{1}{T_{ref}} - \frac{1}{T} \right) \right]} \quad (3)$$

$$I_p = \frac{V_{PV} + I_{PV}R_S}{R_p} \quad (4)$$

The output current of the Photovoltaic model is given as [7]

$$I_{PV} = N_p I_{PH} - N_p I_0 \left[ e^{\frac{q(V_{PV} + I_{PV}R_S)}{nKT}} - 1 \right] - I_p \quad (5)$$

**Table 1.** Parameters of the Kyocera Solar KD215GX-LPU PV panel used in this task.

Quantity	Value
$V_{mpp}$	26.6 V
$I_{mpp}$	8.09A
$P_{mpp}$	215.194W
$V_o$	33.2V
$I_{sc}$	8.78A
$K_i$	$(0.02 \pm 0.015) \% / ^\circ C$
$K_v$	$-(93 \pm 10) mV / ^\circ C$
$N_s$	54

Where :

$V_{PV}$ : photovoltaic voltage,  $I_0$ : diode reverse saturation current,  $I_{PV}$ : photovoltaic cell output current,  $I_{PH}$ : photogeneration current,  $I_{SC}$ : short-circuit cell current,  $I_D$ : diode current,  $k$ : The constant of Boltzmann that equal to  $((1.38) * 10^{-23} J / K)$ ,  $q$ : the charge of electrons ( $1.602 * 10^{-19} C$ ),  $R_S$ : Series resistance of solar cells,  $R_p$ : Parallel resistance of solar cells,  $n$  is diode emission coefficient,  $T$  is Kelvin unit Ambient temperature,  $T_{ref}$  the reference absolute temperature,  $E_g$ : the silicon bandgap energy (1~3) eV,  $K_i$ : the current temperature coefficient in a short circuit and  $I_{do}$ : Reverse current of the diode [8].

In the ideal case,  $R_s$  is equal to zero and  $R_p$  is infinite. Industrialists try to reduce the effects of both resistances to improve the product [8].

### 3. DC-DC Boost Converter

The DC-DC boost converter is the essence of the MPPT strategy. A Boost converter is used to convert the solar array's maximum power to the load side and make sure that the maximum power has been transferred. A boost converter is utilized to change the output voltage by setting the duty cycle to get the solar array's maximum power in this paper, as shown in Figure 2. The MPPT algorithm is utilized to rule the duty cycle of the boost converter [9]. Boost converters can be designed and modeled using the following formulas:

$$V_{out} = \frac{DV_{in}}{1-D} \tag{6}$$

$$L_{min} = \frac{(1-D)^2DR}{2f} \tag{7}$$

$$C_{min} = \frac{DV_o}{V_rRf} \tag{8}$$

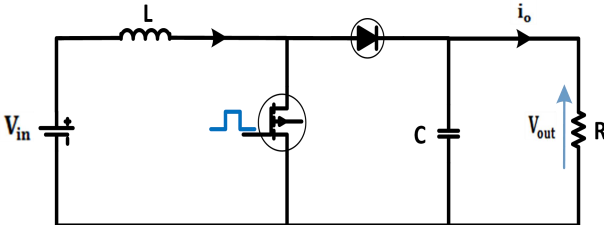


Fig. 2. DC-DC Boost Converter

Where:

D: the duty cycle; Vin: input voltage; Vo: output voltage; Vr: ripple voltage; F: the switching, frequency, and R is the load impedance

4. The Incremental Conductance (IC) algorithm

The MPPT technology is utilized from solar panels to get maximum power efficiency. PV modules are not constantly concerning the power supply and the V-I characteristics are non-linear making them difficult to use to power the load. This is achieved by using a DC-DC boost converter that can be controlled by changing the duty cycle of the entire MPPT algorithm. Over the last few years, many techniques have relied on MPP tracking. Many MPPT algorithms are reported[9][10]. In our PV generation system, we used the IC algorithm. The IC algorithm is the most well-known used algorithm due to its low cost, good execution, and simple implementation. A flow chart for the IC MPPT algorithm is seen in Figure 3 [3].

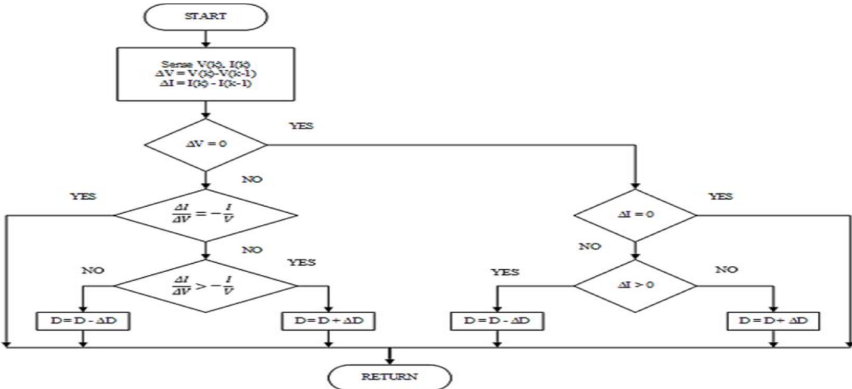


Fig. 3. The P&O MPPT algorithm

5. Three-phase Voltage Source Inverter (VSI)

The circuit of a 3-phase, 3-level NPC inverter is seen in Figure4 . The 3-level NPC inverter is made up of IGBTs and diodes having breakdown voltages lower than the DC voltage source. Since the breakdown voltage is lower in these systems, the losses are lower. As

a result, the efficiency of the three-level inverter is higher than that of the two-level inverter[11].

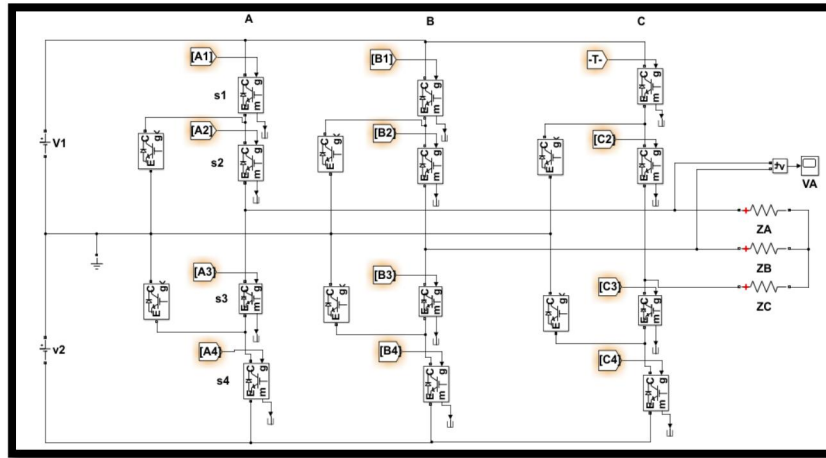


Fig. 4. The inverter

## 6. Three-Phase Space Vector Pulse Width Modulation Technique(SVPWM)

Space Vector Modulation (SVM) was evolved as a vector approach to PWM for 3-phase inverters. It is a more proceeding technique for begetting a sine wave that supplies a loud voltage to the motor with minimum total harmonic distortion [12]. The major aim of any modulation technique is to get changing output owing a top fundamental component with lower harmonics[13].The Space Vector PWM technique is utilized to generate the switching control signals to be supplied to the 3-phase inverter. The SVPWM inverter is utilized to present a 15% rise in the dc-link voltage employment and minimum output harmonic distortions in comparison with the conventional sinusoidal PWM inverter. The SVPWM inverter is the voltage/frequency control method that depends on the SVM Technique[14]

T-type NPC inverter can utilize the same modulation technique as a three-level NPC inverter because the switching scheme will be the same. There are six sectors in a three-level inverter. There are four regions in each sector. Here, a Space Vector Modulation approach with a minimum dwelling time measurement is utilized. The calculations for one sector's dwell time are complete, and the results can be applied to other sectors by measuring a new reference vector angle between 0 and 60°.The principle of Space Vectors is utilized to produce the gating pulses of the switches in SVM. For SVPWM execution, the phase voltages provided by the T-type NPC are converted into Space Vectors[15]. Figure 5 shows a space vector diagram.

Let  $V\alpha$ , and  $V\beta$  by using Clark's transformation[16].

$$\begin{bmatrix} V\alpha \\ V\beta \end{bmatrix} = \frac{2}{3} \begin{bmatrix} 1 & -\frac{1}{2} & -\frac{1}{2} \\ 0 & \frac{\sqrt{3}}{2} & -\frac{\sqrt{3}}{2} \\ \frac{1}{2} & \frac{1}{2} & \frac{1}{2} \end{bmatrix} \begin{bmatrix} v_A \\ v_B \\ v_C \end{bmatrix} \quad (9)$$

Then that calculates  $|\bar{V}ref|$  and  $\alpha$  from Figure 6 as following.

$$|\bar{V}ref| = \sqrt{V\alpha^2 + V\beta^2} \quad (10)$$

$$\alpha = \tan^{-1} \left( \frac{V\beta}{V\alpha} \right) \tag{11}$$

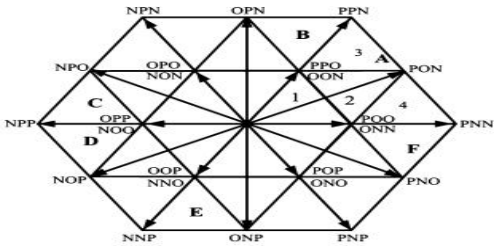


Fig. 5. Voltage sectors, and Switching vectors

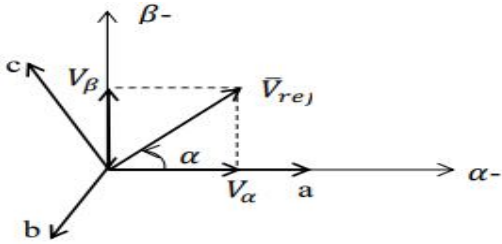


Fig. 6. Reference for voltage vector

The procedure for getting Simulink model for SVPWM Three-level inverter as shown in Figures 21 and 22.

- A. Determination of sector.
- B. Selection of the region.
- C. Calculation of on time for each sector.
- D. Generating Symmetrical PWM.

**A. Determination of sector :** Any reference vectors sector of operation can be calculated by [17]:

$$\text{Sector} = \text{int} (\alpha/60) + 1 \tag{12}$$

**B. Selection of the region:** Modulation that is linear As shown in Figure 7, the length of the reference vector is divided into two sections, m1, and m2 [18]. According to the following, the  $V_{Ref}$  is located in a different region as Table 2 [19].

$$m_n = \sqrt{3}m_a \tag{13} \qquad m_2 = a = \frac{b}{\sin \frac{\pi}{3}} = \frac{2}{\sqrt{3}} b \tag{15}$$

$$m_1 = d - c = m_n \frac{2}{\sqrt{3}} \left[ \sin \left( \frac{\pi}{3} - \alpha \right) \right] \tag{14} \qquad m_2 = 2 * m_n * \frac{\sin \alpha}{\sqrt{3}} \tag{16}$$

$$m_a = \text{modulation index} = \frac{\sqrt{3}V_{Ref}}{V_{dc}} \tag{17}$$

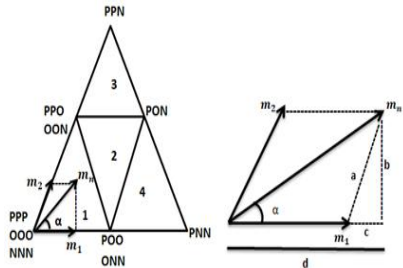


Fig. 7. Calculation of m1 and m2 in sector

Table 2. The  $V_{Ref}$  is located in a different region

Region	Length
1	$m_1, m_2$ and $(m_1 + m_2) < 0.5$
2	$m_1 < 0.5, m_2 < 0.5$ and $(m_1+m_2) > 0.5$
3	$m_2 > 0.5$
4	$m_1 > 0.5$

**C. Calculation of on time for each sector :** Assuming that the reference voltage vector  $V_{Ref}$  remains in region 2, it can be composed of the voltage vectors  $V_1, V_2,$  and  $V_8$  as shown in Figure 8. During the sampling time, the output voltage of three consecutive voltage vectors

should reflect the reference voltage  $T_S$ . As a result, the voltage vectors on-time equations can be written as [20]:

$$\vec{V}_{ref} T_S = \vec{V}_1 T_A + \vec{V}_8 T_B + \vec{V}_2 T_C \quad (18)$$

$$\vec{V}_1 = \frac{v_{dc}}{3} e^{-i0} = \frac{1}{2} \quad (19)$$

$$\vec{V}_2 = \frac{v_{dc}}{3} e^{-i\frac{\pi}{3}} = \frac{1}{2} e^{-i\frac{\pi}{3}} \quad (20)$$

$$\vec{V}_8 = \frac{v_{dc}}{3} e^{-i\frac{\pi}{6}} = \frac{\sqrt{3}}{2} e^{-i\frac{\pi}{6}} \quad (21)$$

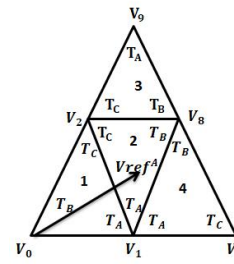


Fig. 8. Vector combination in sector A

$$T_A + T_B + T_C = T_S \quad (22)$$

$$\frac{V_{ref}}{\frac{2}{3}V_{dc}} e^{j\alpha} T_S = \frac{1}{2} T_A + \frac{\sqrt{3}}{2} e^{-i\frac{\pi}{6}} T_B + \frac{1}{2} e^{-i\frac{\pi}{3}} T_C \quad (23)$$

V1 has a dwell time of  $T_A$ , V8 has a dwell time of  $T_B$ , and V2 has a dwell time of  $T_C$ . The sampling period is  $T_S$ . The on-time of the voltage vector can be determined utilizing the above equation as follows [21], as shown in Table 3:

$$T_A = T_S - 2 K \sin \alpha \quad (24)$$

$$T_B = 2 K \sin \left( \frac{\pi}{3} + \alpha \right) - T_S \quad (25)$$

$$T_C = T_S - 2 K \sin \left( \frac{\pi}{3} - \alpha \right) \quad (26)$$

$$K = \frac{2}{\sqrt{3}} m_n T_S \quad (27)$$

The switching sequence must be determined after the times have been calculated. The switching sequence may be set to achieve certain optimal objectives, such as the lowest switching loss or the lowest THD. In the regions of sector A, the switching sequences are as seen in Table 4 [22]:

Table 3. On times in sector A

Region	On-time		
	$T_A$	$T_B$	$T_C$
1	$2 K \sin \left( \frac{\pi}{3} - \alpha \right)$	$T_S - 2 K \sin \left( \frac{\pi}{3} + \alpha \right)$	$2 K \sin \alpha$
2	$T_S - 2 K \sin \alpha$	$2 K \sin \left( \frac{\pi}{3} + \alpha \right) - T_S$	$T_S - 2 K \sin \left( \frac{\pi}{3} - \alpha \right)$
3	$2 K \sin \alpha - T_S$	$2 K \sin \left( \frac{\pi}{3} - \alpha \right)$	$2 T_S - 2 K \sin \left( \frac{\pi}{3} + \alpha \right)$
4	$2 T_S - 2 K \sin \left( \frac{\pi}{3} + \alpha \right)$	$2 K \sin \alpha$	$2 K \sin \left( \frac{\pi}{3} - \alpha \right) - T_S$

Table 4. A switching sequence arranged in the regions of sector A

Region	The switching sequences
1	PPO-POO-OOO-OON-ONN and return
2	PPO-POO-PON-OON-ONN and return
3	PPO-PPN-PON-OON and return
4	POO-PON-PNN-ONN and return

**D. Generating Symmetrical PWM:** The PWM generator that activates the switch can generate the PWM signals. As an example, the region 2 switching sequence can be organized as shown in Figure 9 to easily generate symmetrical PWM signals. Every phase contains three voltage



levels, as indicated by the topology's name, and is generated by two PWM generators. The waveform can be divided into two 2-level waveforms utilizing phase B in Figure 9, which could be simply created utilizing two PWM generators [23]. Switching sequences structured in a symmetrical pattern can be utilized to set the PWM fired time to every switch in sector A, as shown in Table 5 [24].

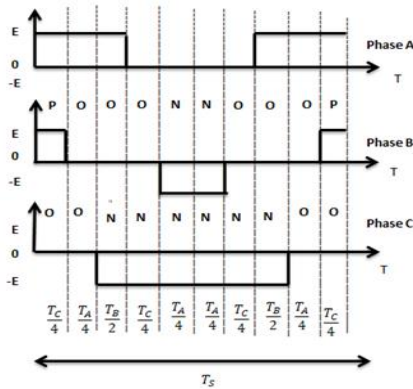


**Fig. 9.** Switching sequence for region 2 in a symmetrical pattern

**Table 5.** Setting the PWM fired time to every switch in sector

Time	Region			
	1	2	3	4
PWM <sub>S1A</sub>	$\frac{T_C}{4} + \frac{T_A}{4}$	$\frac{T_C}{4} + \frac{T_A}{4} + \frac{T_B}{2}$	$\frac{T_S}{2} - \frac{T_C}{4}$	$\frac{T_S}{2} - \frac{T_A}{4}$
PWM <sub>S2A</sub>	$\frac{T_S}{2}$	$\frac{T_S}{2}$	$\frac{T_S}{2}$	$\frac{T_S}{2}$
PWM <sub>S1B</sub>	$\frac{T_C}{4}$	$\frac{T_C}{4}$	$\frac{T_C}{4} + \frac{T_A}{2}$	0
PWM <sub>S2B</sub>	$\frac{T_S}{2} - \frac{T_A}{4}$	$\frac{T_S}{2} - \frac{T_A}{4}$	$\frac{T_S}{2}$	$\frac{T_A}{4} + \frac{T_B}{2}$
PWM <sub>S1C</sub>	0	0	0	0
PWM <sub>S2C</sub>	$\frac{T_S}{2} + \frac{T_A}{4} + \frac{T_C}{4}$	$\frac{T_C}{4} + \frac{T_A}{4}$	$\frac{T_C}{4}$	$\frac{T_A}{4}$

They assume that reference vector A remains in sector A's region 2, and the vector A is rotated 60 degrees clockwise to generate reference vector B, as shown in Figure 10.

$$(V_{ref})^A = \frac{2}{3} (V_A + V_B e^{j\frac{2\pi}{3}} + V_C e^{-j\frac{2\pi}{3}}) \tag{28}$$

As a result, the reference vector  $(V_{ref})^B$  can be written as follows:

$$(V_{ref})^B = (V_{ref})^A * e^{j\frac{\pi}{3}} = \frac{2}{3} (-V_B - V_C e^{j\frac{2\pi}{3}} - V_A e^{-j\frac{2\pi}{3}}) \tag{29}$$

The reference vector is rotated to sector A when it is in any of the other sectors (n=1, 2, 3, 4, 5). In other sectors, Table 6 demonstrates how to generate the corresponding comparison vector[25].

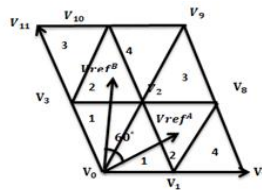


**Fig. 10.** Two vectors with 60° shifting in the sector A and B

**Table 6.** Relationships of phase voltage constructing the reference vectors in six sectors

sectors	Phase voltage A	Phase voltage B	Phase voltage C
A	$V_A$	$V_B$	$V_C$
B	$-V_B$	$-V_C$	$-V_A$
C	$V_C$	$V_A$	$V_B$
D	$-V_A$	$-V_B$	$-V_C$
E	$V_B$	$V_C$	$V_A$
F	$-V_C$	$-V_A$	$-V_B$



As a result, vectors A and B of the same length are located in sectors A and B's region 2 respectively. The reference vector  $(V_{ref})^A$  can be composed of vectors  $V_1, V_2$  and  $V_8$ , as described in Section II, and the on times can be determined utilizing expression (30). The reference vector  $(V_{ref})^B$ , but on the other hand, can be composed of the vectors  $V_2, V_8$  and  $V_{10}$ , whose on times can also be given as:

$$\overline{(V_{ref})^B} T_S = \overline{V_2} T_A + \overline{V_{10}} T_B + \overline{V_8} T_C \quad (30)$$

When PWM signals are exchanged within two corresponding phases, phase voltage shifting is simplified. Although, as shown in Figure (3.30), phase voltage reversing can be accomplished by mirroring the PWM signals of the upper arm switches with those of the lower arm. Assume that the switching state is P, which means that the switches are both  $S_1$  and  $S_2$  on and the switches are both  $S_3$  and  $S_4$  off. After mirroring, the switching state is P while being the switching state is N and the switches are  $S_1$  and  $S_2$  off and switches  $S_3$  and  $S_4$  are on.

When the switching state is N, the same effect occurs. By mirroring, when the switching state is O, the switching state remains O. As a result of this, the phase voltage can be reversed. Table 7 illustrates the relationship between  $S_1$  and  $S_2$  on times before and after mirroring. The calculation flow for six sectors, as shown in Figure (4.34), can be mapped into sector A using a simplified algorithm. The simplified calculation flow will greatly reduce the hardware requirements for hardware implementation as compared to the traditional calculation flow implemented in Section I

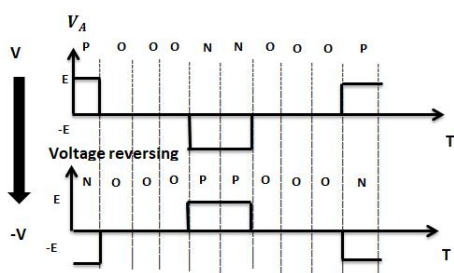


**Fig. 11.** Phase voltage reversing by mirroring PWM signals.

**Table 7.** Relationship of on times of  $S_1$  and  $S_2$  before and after mirroring

Phase voltage	On times	
	$S_1$	$S_2$
V	PWM $S_{1B}$	PWM $S_{2B}$
-V	$\frac{T_S}{2} - \text{PWM } S_{2B}$	$\frac{T_S}{2} - \text{PWM } S_{1B}$

## 7. Simulation Results

As shown in Figure 12, the PV system with the IC controller MPPT method and an SVPWM control scheme for a 3-phase PWM inverter is implemented in the Matlab / Simulink software package. The Simulink model of the PV module is designed according to the mathematical formulas is shown in Figure 13. The Kyocera Solar KD215GX-LPUPV module has the characteristics shown in Table 1. The Simulink models of the boost converter and controller are shown in Figures 14. The boost converter inductance and capacitor values are 0.01MH and 700 $\mu$ F respectively while the output load value is 78 ohms.

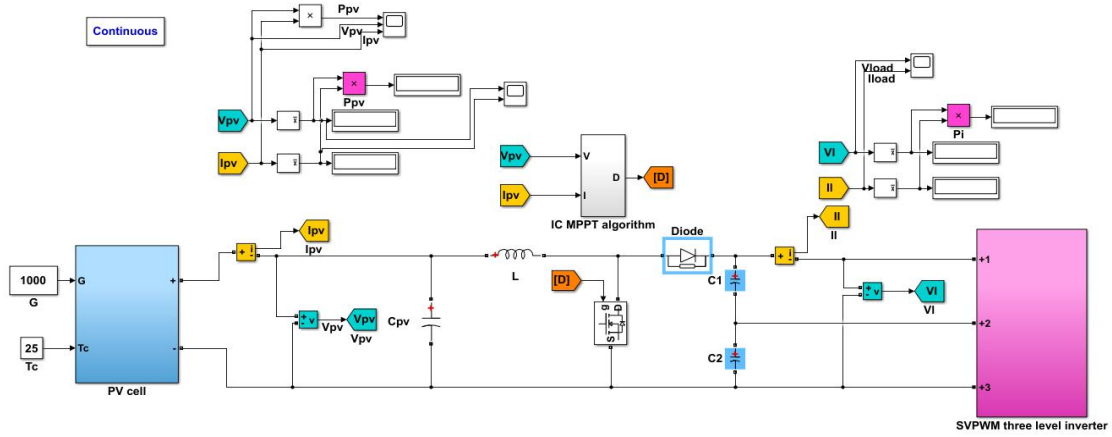


**Fig. 12.** The Simulink model for The PV system with an IC controller MPPT algorithm and SVPWM control for 3ph source PWM inverter

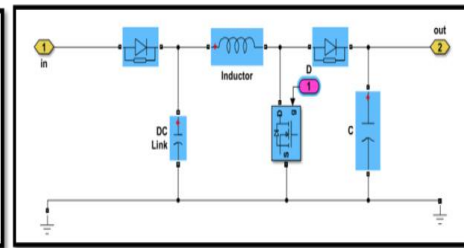
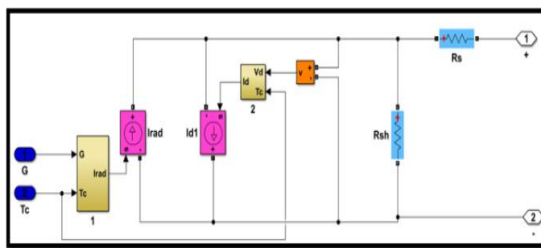


**Fig. 13.**The Simulink model for the PV system **Fig. 14.**The Simulink model for the Boost converter

The operation test of the Photovoltaic system in simulation including the Photovoltaic system response, The outputs of the boost converter under different values in irradiance and temperature are shown in Figures 15, 16, 17, 18,19, and 20. For example, If the load is connected directly to the PV panel at  $G = 1000 \text{ w/m}^2$  and  $T = 25^\circ \text{ C}$ , the power is 213.9 Watts, but for the same load when connected to PV via a boost converter-based MPPT algorithm, the power is 210 Watts. Therefore, the IC controller is efficient at extracting MPPT in the context of temperature and irradiation changes.

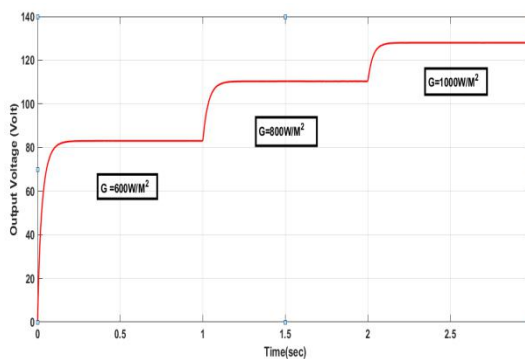


**Fig. 15.** The output voltage responses for boost converter at  $T = 25^\circ \text{ C}$

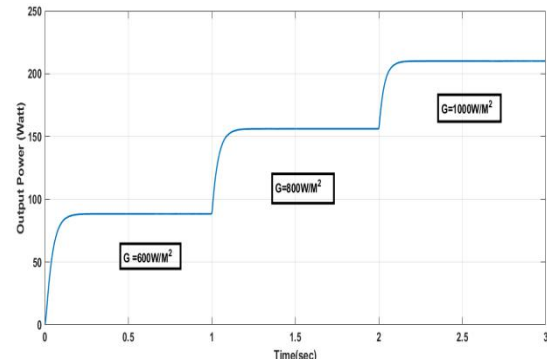


**Fig. 16.** The output power responses for boost converter at  $T = 25^\circ \text{ C}$

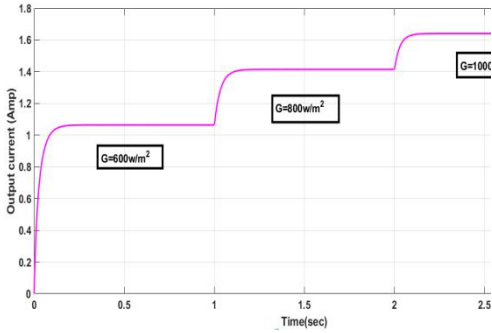


Fig. 17. The output current responses for boost converter at T =25 °C

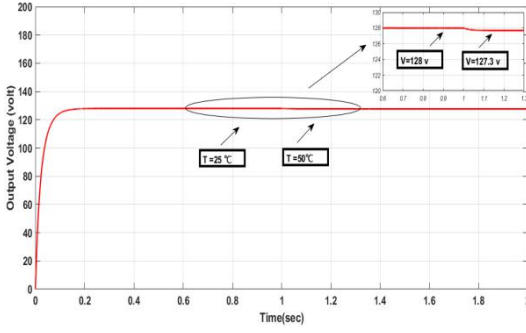


Fig. 18. The boost converter output voltage response for changing Temperature at G=1000 w/m²

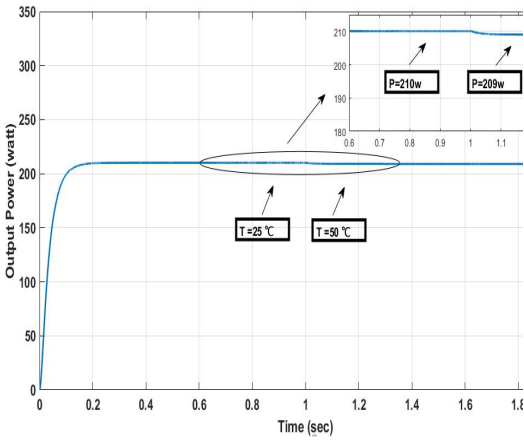


Fig. 19. The boost converter output power response for changing temperature at G=1000 w/m²

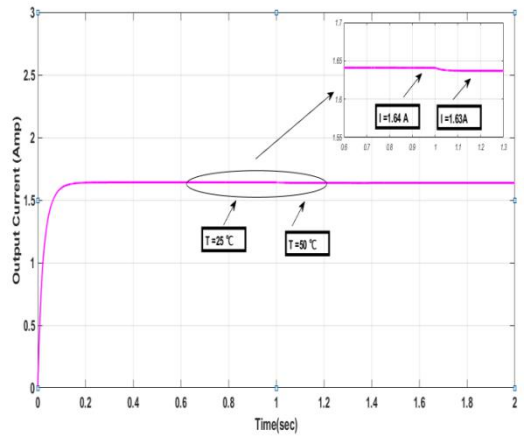
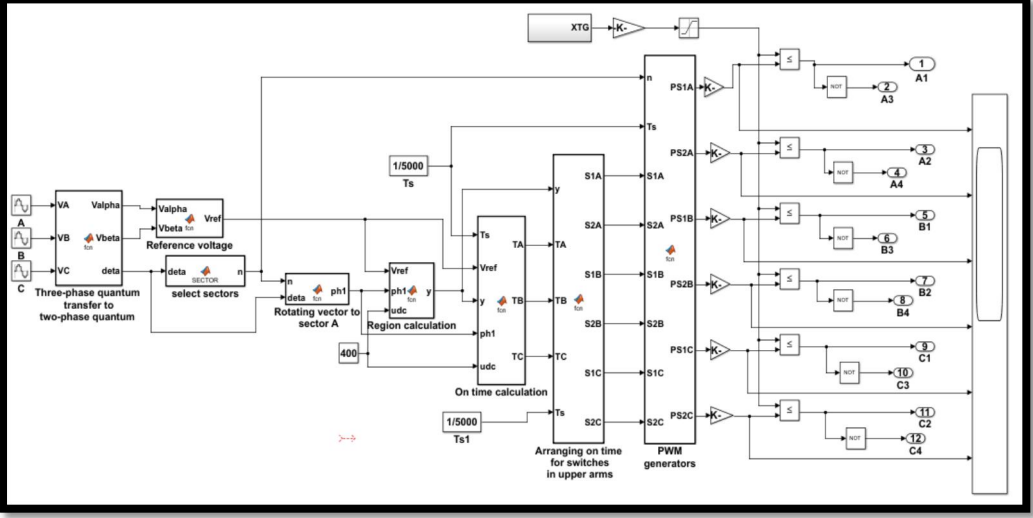
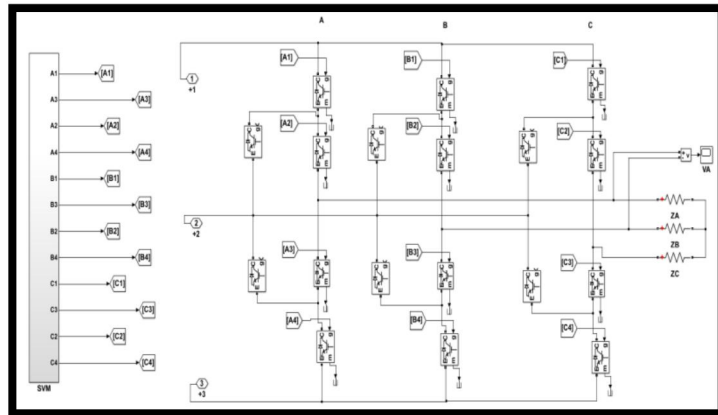


Fig. 20. The boost converter output current response for changing temperature at G=1000 w/m²

The output of the SVPWM is produced from the Simulink model illustrated in Figure 21 in which including positioning the reference vector according to the fundamental frequency ( $f = 50 \text{ Hz}$ ), sampling frequency ( $f_s = 10 \text{ kHz}$ ). By calculating the switching sequence time of different switching states according to the sector of the reference vector. Figure 22 shows a Simulink block diagram model of the inverter.



**Fig. 21.** The Simulink block diagram for SVPWM Three-level inverter



**Fig. 22.** The simulation block diagram for the SVPWM Three-level inverter

The output voltages of SVPWM in case of  $T = 25\text{ }^{\circ}\text{C}$  and  $G = 1000\text{ w/m}^2$  is shown in Figure 23. The output voltages of SVPWM in case of changing the irradiance at  $T = 25\text{ }^{\circ}\text{C}$  are shown in Figure 24 and the output voltages at  $T = 50\text{ }^{\circ}\text{C}$  are shown in Figure 25. The THD of output line voltage for  $G = 1000\text{ w/m}^2$  equal 30.26% ,  $G = 800\text{ w/m}^2$  equal 30.25% ,and  $G = 600\text{ w/m}^2$  equal 30.25% are seen in Figures 26, 27, and 28 at  $T = 25\text{ }^{\circ}\text{C}$  .

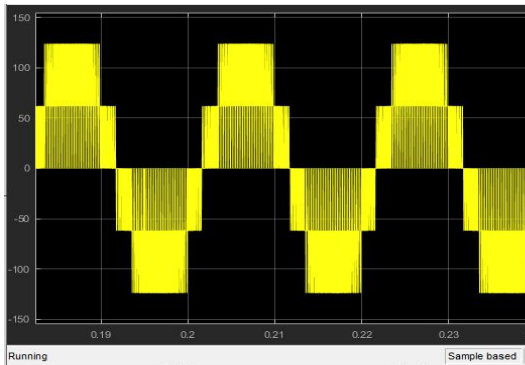


**Fig. 23.** The output voltages for SVPWM for  $G = 1000\text{ w/m}^2$  and  $T = 25\text{ }^{\circ}\text{C}$

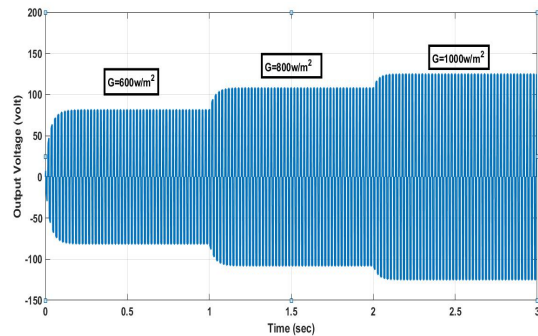


**Fig. 25.** The output voltages for SVPWM for different irradiation at  $T = 50\text{ }^{\circ}\text{C}$

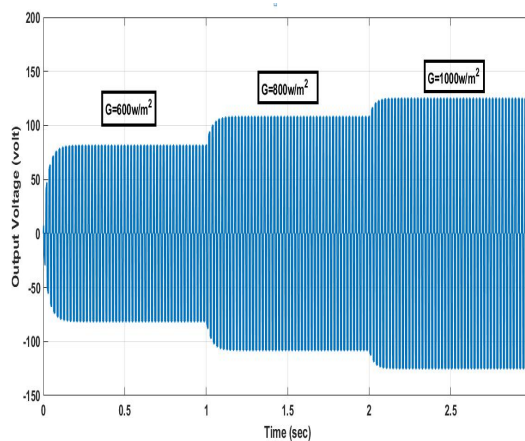


**Fig. 24.** The output voltages for SVPWM for different irradiation at  $T = 25\text{ }^{\circ}\text{C}$

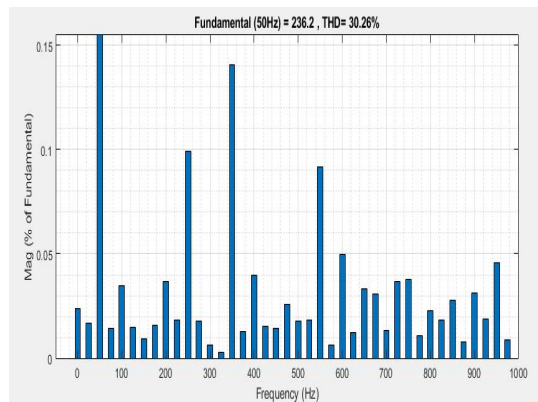


**Fig. 26.** The THD of output line voltage for SVPWM for  $G = 1000\text{ w/m}^2$

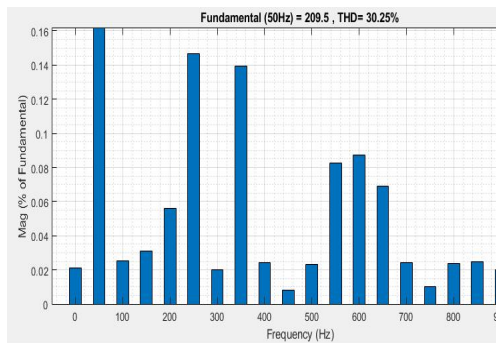


**Fig. 27.** The THD of output line voltage for SVPWM for  $G= 800 \text{ w/m}^2$

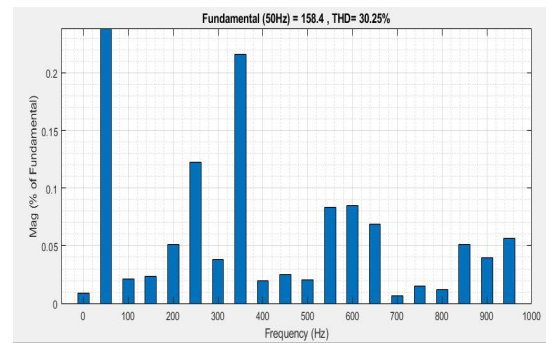


**Fig. 28.** The THD of output line voltage for SVPWM for  $G= 600 \text{ w/m}^2$

## 8. Conclusion

In this paper, a stand-alone Photovoltaic power generation system is proposed. The proposed design depends on IC MPPT algorithm and SVPWM control method for a 3-phase voltage source PWM inverter. The IC MPPT algorithm is implemented in Matlab / Simulink. The simulation results show that the IC MPPT algorithm can simultaneously get better performance of the dynamic and steady-state performance of Photovoltaic systems. At the same time, the output result of the inverter using the SVPWM control strategy have better power quality. The results also show that the proposed Photovoltaic system has a reliable and effective response under variation atmospheric conditions. Therefore, a stand-alone Photovoltaic power generation system based on the IC MPPT method for a 3-phase voltage source pulse width modulation inverter and SVPWM control is practical and effective. The designed system produces the ability to operate at lower switching frequencies with less  $dv/dt$  the voltage stress on the switching device. Space vector pulse width modulation is the best selection of inverter switching states that makes optimization of switching patterns and improves the DC link voltage employment. This is more efficient than other traditional pulse width modulation methods.

## Reference:

- [1] A. Pandey, N. Dasgupta, and A. K. Mukerjee, "High-performance algorithms for drift avoidance and fast tracking in solar MPPT system," *IEEE Trans. Energy Convers.*, vol. 23, no. 2, pp. 681–689, 2008, doi: 10.1109/TEC.2007.914201.
- [2] P. Shaw, "Modelling and analysis of an analogue MPPT-based PV battery charging system utilising DC-DC boost converter," *IET Renew. Power Gener.*, vol. 13, no. 11, pp. 1958–1967, 2019, doi: 10.1049/iet-rpg.2018.6273.
- [3] W. I. Hameed, A. L. Saleh, B. A. Sawadi, Y. I. A. Al-Yasir, and R. A. Abd-Alhameed, "Maximum power point tracking for photovoltaic system by using fuzzy neural network," *Inventions*, vol. 4, no. 3, 2019, doi: 10.3390/inventions4030033.
- [4] B. M. Hasaneen and A. A. E. Mohammed, "Design and simulation of DC/DC boost converter," *2008 12th Int. Middle East Power Syst. Conf. MEPCON 2008*, pp. 335–340, 2008, doi: 10.1109/MEPCON.2008.4562340.
- [5] M. Chen and D. Sun, "A unified space vector pulse width modulation for dual two-level inverter system," *IEEE Trans. Power Electron.*, vol. 32, no. 2, pp. 889–893, 2017, doi: 10.1109/TPEL.2016.2585223.
- [6] A. M. Dakhil, A. R. Hussein, and A. L. Saleh, "Transformer-less Single-phase Inverter



- Based on SPWM Technique for Standalone PV Application,” *Solid State Technol.*, vol. 63, no. 3, pp. 4088–4101, 2020.
- [7] P. K. Pathak and A. K. Yadav, “Design of battery charging circuit through intelligent MPPT using SPV system,” *Sol. Energy*, vol. 178, no. July 2018, pp. 79–89, 2019, doi: 10.1016/j.solener.2018.12.018.
- [8] S. Wadhankar and B. Charjan, “Design and Simulation of Photovoltaic Water Pumping System,” no. September, pp. 83–92, 2019, doi: 10.1007/978-981-13-6148-7\_9.
- [9] A. Badis, M. H. Boujmil, and M. N. Mansouri, “A comparison of global MPPT techniques for partially shaded grid-connected photovoltaic system,” *Int. J. Renew. Energy Res.*, vol. 8, no. 3, pp. 1442–1453, 2018.
- [10] M. A. Eltawil and Z. Zhao, “MPPT techniques for photovoltaic applications,” *Renew. Sustain. Energy Rev.*, vol. 25, pp. 793–813, 2013, doi: 10.1016/j.rser.2013.05.022.
- [11] A. Zorig, M. Belkheiri, and S. Barkat, “Control of three-level T-type inverter based grid connected PV system,” *13th Int. Multi-Conference Syst. Signals Devices, SSD 2016*, no. 1, pp. 66–71, 2016, doi: 10.1109/SSD.2016.7473723.
- [12] I. Chaib, E. M. Berkouk, J.-P. Gaubert, M. Kermadi, N. Sabeur, and S. Mekhilef, “An Improved Discontinuous Space Vector Modulation for Z-Source Inverter With Reduced Power Losses,” *IEEE J. Emerg. Sel. Top. Power Electron.*, vol. 9, no. 3, pp. 3479–3488, 2020, doi: 10.1109/jestpe.2020.3002684.
- [13] K. Kalpana and S. Sankar, “Comparison of Three Phase Dc/Ac Inverter and Two Level Dc/Ac Inverter Based on Space Vector Pwm,” no. November, 2020, [Online]. Available: <https://seyboldjournal.com/wp-content/uploads/2020/10/COMPARISON-OF-THREE-PHASE-DCAC-INVERTER-AND-TWO-LEVEL-DCAC-INVERTER-BASED-ON-SPACE-VECTOR-PWM.pdf>.
- [14] V. Janaki Ramaiah and S. Keerthipati, “Hybrid PWM Scheme for Pole-Phase Modulation Induction Motor Drive Using Carrier-Based Hexagonal and Octadecagonal SVPWM,” *IEEE Trans. Ind. Electron.*, vol. 67, no. 9, pp. 7312–7320, 2020, doi: 10.1109/TIE.2019.2946537.
- [15] Z. Gao, Q. Ge, Y. Li, L. Zhao, and B. Zhang, “A SVPWM method with reduced switching frequency suitable for high power three-level NPC rectifiers,” *2019 IEEE Energy Convers. Congr. Expo. ECCE 2019*, pp. 4824–4831, 2019, doi: 10.1109/ECCE.2019.8912918.
- [16] M. Biswas, S. Podder, and Z. R. Khan, “Modified H-Bridge multilevel inverter for photovoltaic micro-grid systems,” *Proc. 9th Int. Conf. Electr. Comput. Eng. ICECE 2016*, pp. 377–380, 2017, doi: 10.1109/ICECE.2016.7853935.
- [17] R. Attia, K. Abdellah, and H. Ahmed, “Space Vector Pulse Width Modulation for Three Phase Cascaded H-Bridge Inverter,” *Proc. 2018 Int. Conf. Appl. Smart Syst. ICASS 2018*, no. November, pp. 1–6, 2019, doi: 10.1109/ICASS.2018.8652080.
- [18] A. A. Kadum, “PWM control techniques for three phase three level inverter drives,” *Telkomnika (Telecommunication Comput. Electron. Control.*, vol. 18, no. 1, pp. 519–529, 2020, doi: 10.12928/TELKOMNIKA.V18I1.12440.
- [19] M. Sajitha and R. Ramchand, “Space Vector PWM Scheme for Three Phase Three Level T-type NPC Inverter,” *2019 2nd Int. Conf. Intell. Comput. Instrum. Control Technol. ICICICT 2019*, pp. 523–528, 2019, doi: 10.1109/ICICICT46008.2019.8993215.
- [20] P. Chamarthi, P. Chhetri, and V. Agarwal, “Simplified Implementation Scheme for Space Vector Pulse Width Modulation of n-Level Inverter with Online Computation of Optimal Switching Pulse Durations,” *IEEE Trans. Ind. Electron.*, vol. 63, no. 11, pp. 6695–6704, 2016, doi: 10.1109/TIE.2016.2586438.
- [21] D. Roy and M. Singh, “A simplified space vector pulse width modulation for three phase three-level diode clamped inverter,” *2017 Int. Conf. Smart Grids, Power Adv. Control Eng. Icspace 2017*, vol. 2018-Janua, pp. 226–230, 2018, doi: 10.1109/ICSPACE.2017.8343433.
- [22] A. A. Yacine, H. Farid, K. Aissa, M. Abdeslam, M. Brahim, and L. Youssef,

- “Implementation of Modified SVPWM for Three-level Inverter Using STM32F4,” *Proc. 2018 3rd Int. Conf. Electr. Sci. Technol. Maghreb, Cist. 2018*, no. January 2019, 2019, doi: 10.1109/CISTEM.2018.8613592.
- [23] C. Piao and J. Y. Hung, “A simplified space vector PWM algorithm for three-level NPC VSI,” *Conf. Proc. - IEEE SOUTHEASTCON*, vol. 2015-June, no. June, 2015, doi: 10.1109/SECON.2015.7132961.
- [24] R. L. Naik and K. B. Hunasikatti, “FPGA Based Implementation of Symmetrical Switching in SVPWM for Three Level NPC Converter,” *Proc. 3rd Int. Conf. Inven. Syst. Control. ICISC 2019*, no. Icisc, pp. 592–597, 2019, doi: 10.1109/ICISC44355.2019.9036409.
- [25] A. A. Yacine, A. A. Noureddine, K. Aissa, and M. Brahim, “Design and implementation of three-level inverter for grid-tied PV systems,” *2017 5th Int. Conf. Electr. Eng. - Boumerdes, ICEE-B 2017*, vol. 2017-Janua, pp. 1–6, 2017, doi: 10.1109/ICEE-B.2017.8191993.





**Dhuha K. Kafaz** was born in Basrah Iraq in 1990. she received the B.S. degree in Electrical Engineering from the University of Basrah in 2013 and M.S. in Electrical Engineering from the Basra Engineering Technical College, Southern Technical University, Iraq in 2020. Her research interests include control , DSP , and Fundamental of Electrical Engineering



## مجلة كلية العراق للهندسة والعلوم التطبيقية

### نظام توليد الطاقة الكهروضوئية يعتمد على خوارزمية MPPT للتوصيل المتزايد وعاكس SVPWM للتطبيقات المستقلة

ضحى كريم<sup>1</sup>

1 كلية العراق الجامعة , قسم هندسة الاتصالات , البصرة , العراق.

البريد الإلكتروني: [Duhakareem249o0ll@gmail.com](mailto:Duhakareem249o0ll@gmail.com)

**الملخص:** تستمر الطاقة المنتجة عند خرج الخلايا الكهروضوئية في التغير بسبب الإشعاع الشمسي ودرجة حرارة البيئة المحيطة بحيث تُظهر الخلايا الكهروضوئية خصائص غير خطية للتيار والجهد. لذلك ، تعتمد نقطة الطاقة القصوى للخلايا الشمسية على كمية الإشعاع الشمسي ودرجة حرارة البيئة. تُستخدم تقنية Maximum Power Point Tracking (MPPT) في الأنظمة الكهروضوئية للاستفادة الكاملة من طاقة الإخراج للخلايا الكهروضوئية. تقترح هذه الورقة طريقة خوارزمية MPPT للتوصيل الإضافي والتي يمكنها في نفس الوقت زيادة سرعة ودقة MPPT. تعتبر وحدة التحكم في العاكس جانباً مهماً آخر من نظام توليد الطاقة الكهروضوئية. يقترح هذا البحث طريقة التحكم في تعديل عرض النبضة المتجهية (SVPWM) لعاكس تعديل عرض النبض ثلاثي الأطوار في أنظمة توليد الطاقة الكهروضوئية. يعتمد نظام توليد الطاقة الكهروضوئية الجديد المستقل على خوارزمية MPPT بطريقة التوصيل التزايدية مع مخطط التحكم في تعديل عرض النبضة متجه الفضااء لعاكس مصدر الجهد ثلاثي الأطوار ويتم تنظيمه في Matlab / Simulink. تظهر نتائج المحاكاة أن النظام الكهروضوئي المستقل المقترح يمكنه تحقيق التنفيذ الممتاز لـ MPPT والحصول على جهد الخرج بجودة عالية. تم اختبار النظام وتنويجه باستخدام وحدة الخلايا الشمسية GX-LPU PV215 Kyocera Solar KD